Published in final edited form as:
J Phys Chem B. 2010 June 17; 114(23): 7777–7783. doi:10.1021/jp102478k.

Evidence for a Quasi-Equilibrium Distribution of States for Bradykinin $[M+3H]^{3+}$ Ions in the Gas Phase

Nicholas A. Pierson, **Stephen J. Valentine**, and **David E. Clemmer***
Department of Chemistry, Indiana University, Bloomington, IN 47405

Abstract

Multidimensional ion mobility spectrometry coupled with mass spectrometry (IMS–IMS-MS) techniques are used to select and activate six different gas-phase conformations of bradykinin $[M+3H]^{3+}$ ions. Drift time distributions as a function of activation voltage show that at low voltages selected structures undergo conformational transitions in what appears to be a pathway dependent fashion. Over a relatively wide range of intermediate activation voltages a distribution of states that is independent of the initial conformation selected for activation (as well as the activation voltage in this intermediate region) is established. This distribution appears to represent an equilibrium distribution of gas-phase structures that is reached prior to the energy required for dissociation. Establishment of a quasi-equilibrium prior to dissociation results in identical dissociation patterns for different selected conformations. A discussion of the transition from solution-like to gas-phase structures is provided.

Keywords

ion mobility; multidimensional; conformational transitions; bradykinin

Introduction

Since the development of electrospray ionization (ESI)1 as a soft ionization source for mass spectrometry (MS), many studies have focused on understanding the structures of the solvent-free macromolecular ions that are produced. 2¯17 A primary aim of this work is to understand the degree to which the population of gas-phase ions resembles the structures that existed in solution prior to ionization. To the extent that ion conformations retain solution-like properties, MS-techniques will be useful in assessing structural information that is relevant to solution. Alternatively, an understanding of structures that arise in the gas-phase, in the absence of solvent will help to delineate the roles of intramolecular and solvent-molecule interactions in defining key structural elements.18

In this paper, we use ion mobility techniques to examine the $[M+3H]^{3+}$ ion of bradykinin (a nonapeptide, with the sequence RPPGFSPFR) produced by ESI. At least six distinct conformations originate from the ESI source. We have selected each of the $[M+3H]^{3+}$ states and measured the activation voltage that is required to induce structural transitions. These studies provide evidence that any of these states is capable of generating an equilibrium distribution of gas-phase structures under the proper activation conditions. Interestingly, the equilibrium distribution that is formed in the gas phase is dominated by only three of the selected states. It appears that even in relatively small molecular systems, a large number of conformations generated by ESI do not reflect the most stable gas-phase structures, which

* To whom correspondence should be addressed: clemmer@indiana.edu.

are formed after ions are activated to a voltage that is near a value that also induces dissociation.

A number of experimental methods have been used to characterize the conformations of biomolecular ions. These include: 1)reactive methods, such as hydrogen-deuterium exchange,3،4،7،9،19،20 measurements of proton-transfer, 14،21،22 molecular adduction experiments, 23-25 and ion-electron as well as ion-ion reactions; 26-28 2) methods that probe ion shape, such as ion energy loss experiments,6،29 microscopy studies of hillocks formed from high energy ion impacts with surfaces,30-32 and IMS measurements of collision cross section;10، 33-37 and, 3)dissociative MS techniques.38-42 Of these techniques, the most direct information about ion shapes is obtained by IMS techniques. 16،43-48 In favorable cases, comparisons of experimental mobilities to those calculated for trial geometries49-51 generated by theory provides relatively detailed insight into the structures of ions.52-55 Mobility measurements have also been used to monitor the structures of electrosprayed ions that were stored in ion traps for varying amounts of time, 56-58 and measurements as a function of drift cell temperature have provided information about the relative stabilities of different conformations.33،59،60

During the last decade, mounting evidence suggests that under some conditions, populations of ions formed by ESI reflect structures that are present in solution. For example, Loo and coworkers found that the higher-order structure of a gas-phase biomolecular ion could be linked to the solution structure using tandem MS experiments.61 Ion mobility results have shown that the distribution of cytochrome *c* and ubiquitin structures that are observed in the gas phase are dependent upon the solution and source conditions used to produce these ions. 62،63 Recently Robinson's and Bowers' groups have examined large non-covalent complexes and suggest that for these large ions, structures in the gas phase may reflect solution conformations as well as structures associated with intermediates that are present in solution.64-66 The present work is the first characterization of an equilibrium distribution of gas phase states prior to dissociation. We have chosen to demonstrate this approach on the bradykinin system because it has been studied extensively.33،67-79 Finally, while this work is at an early stage, it is anticipated that over time, these types of studies will help to clarify whether ion distributions reflect solution- or gas-phase structures.

Experimental Methods

General

IMS theory43-45،49-51 instrumentation,58،80-87 and techniques16،46-48 are discussed in detail elsewhere. In this study, experiments were performed on a home-built ion mobility spectrometer coupled to a time-of-flight (TOF) mass spectrometer (Figure 1), described previously.58،86،87 Briefly, positively charged bradykinin (Sigma, St. Louis, MO) ions were produced by ESI of a 9.4 μM solution in 49:49:2 (% volume) water:methanol:acetic acid. Ions are focused and accumulated in a Smith-geometry ion funnel (F1),88 and pulsed into the drift tube with a 150 μs-wide electrostatic gate (G1). The drift tube (D1 and D2) contains ~3 Torr He buffer gas at 300 K and is operated under a uniform electric field (9.6 $V \cdot cm^{-1}$), allowing ions to separate on the basis of their mobilities. A funnel (F2) in the middle of the drift tube serves to radially focus the diffuse ion packet, and also consists of an electrostatic gate (G2) and activation region (IA2). Following separation through D2, ions are again radially focused through funnel F3. Ions exit the drift tube through a differentially pumped region and are orthogonally accelerated into a field-free flight tube for TOF mass analysis.

Two different instrumental modes were used in this experiment: one-dimensional (IMS-MS), and two-dimensional (IMS–IMS-MS). For IMS-MS experiments, the field in G2 is

maintained at the drift field such that all mobility separated ions through the first drift region (D1) are allowed to pass into the second drift region (D2). Under the IMS-MS mode of operation, D1 and D2 comprise a single, ~1.8-meter drift tube.

Selection and activation

An important part of the work described below involves the selection, activation and subsequent separation of ions (i.e., IMS-IMS) experiments. We have described the instrumentation for these types of studies in detail previously.[58,86,87] Briefly, when a high field is applied across the ion activation region, entering ions undergo energizing collisions with the buffer gas and are heated. As the ions leave the activation region they rapidly equilibrate to the temperature of the buffer gas.

In these experiments, D1 and D2 are operated as two independent drift regions of 0.84 m and 0.98 m, respectively. A mobility selection is obtained after ions pass through D1 by applying a delay pulse at G2 (triggered by the initial pulse at G1). A narrow packet of ions is allowed to pass through G2 by lowering a repulsive potential (16 V) for 25 μs. Ions entering the gate region before or after the transmission pulse is applied are neutralized by a Ni mesh grid (90% transmittance) on the first electrostatic lens of G2. Those mobility-selected ions that continue through F2 can be collisionally activated in the IA2 region prior to subsequent separation through the D2 region.

The activation region IA2 is comprised of two lenses ~0.3 cm apart. For selection with no activation, the field between the two lenses comprising IA2 is held consistent with the ~12 $V \cdot cm^{-1}$ DC field through F2. These field conditions are defined as having an activation of 0 V, such that ion activation is the application of voltage at IA2 resulting in a field greater than 12 $V \cdot cm^{-1}$. Thus, an activation voltage of 70 V corresponds to a field strength of ~233 $V \cdot cm^{-1}$.

Calculating cross section distributions

In the case of a uniform electric field, drift time distributions can be converted to a collision cross section scale using Equation 1:45

$$\Omega = \frac{(18\pi)^{1/2}}{16} \frac{ze}{(k_b T)^{1/2}} \left[\frac{1}{m_I} + \frac{1}{m_B} \right]^{1/2} \frac{t_d E}{L} \frac{760}{P} \frac{T}{273.2} \frac{1}{N} \quad (1)$$

where ze, k_b, m_I, and m_B are the ion's charge, Boltzmann's constant, the mass of the ion, and the mass of the buffer gas, respectively; t_D, E, and L correspond to the ion's drift time, the electric field strength, and the drift length, respectively; P, T, and N are the pressure, temperature, and neutral number density (at STP) of the buffer gas, respectively. The current instrument contains two funnels (F2 and F3) in the drift region, which are operated at a higher drift field field (12 $V \cdot cm^{-1}$) than the drift regions and also contain RF confinement fields. Because a uniform drift field is not applied across the entire drift tube, cross sections are determined by measuring the time required for ions to travel through the uniform field region (from G1 to G2). That is, one determines the selection time required to transmit a single conformer. The selection time, and the length from G1 to G2 (71.3 cm) are substituted in Equation 1 as t_d and L, respectively. Once absolute values of the cross sections for ions within a specific peak are determined (with no activation), these values are then used to generate a calibrated cross section distribution, where all drift times are converted to a calculated cross section. The reproducibility of this approach is excellent. Typically, cross sections for any two measurements agree within ~1% (relative uncertainty).47

Results and Discussion

Determining collision cross sections for bradykinin $[M+3H]^{3+}$ ions formed by direct ESI

A nested drift time(*m*/*z*) distribution recorded upon electrospraying bradykinin is shown in Figure 2. Under the conditions that are employed, this spectrum is dominated by the $[M+2H]^{2+}$ and $[M+3H]^{3+}$ charge states. The drift time distribution for the $[M+3H]^{3+}$ ions, overlaid above the corresponding 2D features, shows at least six distinct reproducible local maxima. We have assigned these features as conformations A through F. Some of the labeled peaks possess shoulders, thus it is possible that the $[M+3H]^{3+}$ drift distribution is made up of many unresolved conformations. For this study, however, we focus on the six selections made, and their resulting distributions upon activation.

It is important to note that we observe no other ions in the region of drift times that are associated with the $[M+3H]^{3+}$ charge state. Thus, upon selection and activation we expect only this charge state to contribute to the new distributions. Figure 2 also shows a blow up of the mass scale. The 0.33 *m*/*z* spacing between the isotopic peaks observed for each of the features requires that all of the ions correspond to the $[M+3H]^{3+}$ charge state. There is no evidence for multiply charged multimers of the same *m*/*z* in this system.[75,89]

Inspection of Figure 2 shows that conformations A, B, and C are more intense, than the features corresponding to the lower-mobility D, E, and F ions. Conformer A is represented by a peak centered around 11.5 ms, and is not baseline resolved from conformer B. Conformer B corresponds to the peak centered around 12.2 ms; and, conformer C corresponds to the peak at 13.0 ms. The low-mobility region of the drift time distribution (~13.5 to 15.5 ms) consists of lower intensity ions, which remain unresolved in the mobility separation. Three selection experiments were performed for the most distinct features in this region, corresponding to isolation of narrow regions designated as conformers D, E, and F having drift times of 13.74, 14.40, and 15.18 ms, respectively.

The drift time distributions can be converted to collision cross section distributions. Here each time point corresponding to the time required for ions to traverse the drift region between G1 and G2, can be used in Equation 1 to calculate a corresponding collision cross section for the $[M+3H]^{3+}$ ions. The cross section distribution obtained for ions generated in the ESI source region is shown in Figure 3. Table 1 lists the collision cross section determined directly from the G1 to G2 measurement as well as the relative abundance (based on peak area) of each dataset feature in the total distribution.

It is interesting that cross sections span a relatively wide range of values, from 269 $Å^2$ to 356 $Å^2$ for conformers A and F, respectively. Values for conformers B (285 $Å^2$) and C (304 $Å^2$) are in agreement with the values 284 $Å^2$ and 293 $Å^2$ obtained previously for the $[M+3H]^{3+}$ charge state.[72,75] The collision cross section obtained for conformer A is slightly smaller than the value of 275 $Å^2$ reported earlier.[75]

Observed conformational changes upon activation

Cross section distributions have been recorded upon selection and activation of each of the six conformations (A through F) over an activation voltage range of 0 to 140 V. Several example distributions for each selected conformer are plotted in Figure 3. At 0 V, selection of conformer A yields a single, narrow peak, indicating that no activation has occurred. Similar distributions are obtained until ~10 V. Upon application of 24 V across the activation region a clear difference in the distribution is observed; although conformer A remains the largest feature (~96% relative abundance) through the second drift separation, conformer B (at 285 $Å^2$) is clearly present (comprising ~4% of the distribution). There is no

evidence for production of other states under these conditions. However, upon increasing the activation voltage to 28 V, it is clear that conformer C (at 305 $Å^2$) is produced.

As can be observed in Figure 3, at higher activation voltages (34 V, 36 V, 38 V, 42 V, and 45 V) the fraction of conformer A continues to decrease. By 38 V, conformers A, B, and C are in roughly equal proportion (33%, 37%, and 30%, respectively). Above 38 V, conformer C becomes the dominant feature in the profile. Proportions of conformers A, B, and C at 70 V activation are 2%, 17%, and 79%, respectively. It is important to note that there are no conditions in which conformer A disappears completely.

Selection of conformer B (having a cross section of 285 $Å^2$) is also plotted above the ESI source distribution in Figure 3. At low activation voltages, the distribution remains dominated by B. At 25 V activation, peaks on each side of B, corresponding to cross sections of 269 and 305 $Å^2$ are observed, indicating the onsets of states A and B. At higher activation voltages (32 V, 38 V, and 40 V) the population of state B decreases. In this case the population of conformer A increases to a maximum of ~2% by 35 V activation (not shown). Conformer C is clearly the dominant feature (56%) in the spectrum obtained at 45 V activation. Conformer B decreases from 30% at 50 V activation to 17% (at 70 V activation). It is important to note that the populations of all three states remain essentially unchanged above ~50 V. Conformers A, B, and C have relative populations of ~2%, ~17% and ~79%, respectively. The distributions obtained at high activation voltages are indistinguishable from the high-voltage distributions obtained from activation of conformer A.

Activation of conformer C shows that this state can also convert to A and B. However, unlike activation of the higher mobility states, under all conditions conformation C dominates the distribution. At the highest activation voltage that is shown (70 V) relative populations of 3%, 17%, and 78% for conformers A, B, and C, respectively are obtained. Effectively, high voltage activation results in the same distribution, regardless of which state was selected.

It is interesting to also consider selection and activation of the lower mobility D, E, and F conformers. Overall, these ions show the same general trend as discussed for A, B, and C above. Selected conformers are converted to increasing fractions of conformers A, B, and C as a function of increasing activation voltage; all experiments converged to the same fraction of A (~2%), B (~17%), and C (~79%) at 70 V. Selected conformers E and F are more stable than conformer D, evidenced by the presence of conformers C and E without activation of conformer D. Additionally, increased activation voltage is needed in order to induce structural transitions back to A, B, and C (Figure 3) as the selected ions became more elongated (D < E < F).

Evidence for formation of a quasi-equilibrium distribution of gas-phase conformations

Figure 3 illustrates the quasi-equilibrium that is established independent of the $[M+3H]^{3+}$ conformation selected. That is, identical distributions are obtained at elevated activation voltages regardless of the initial conformation. This phenomenon has been further investigated in the datasets collected at several different pressures. While the exact activation voltage varies somewhat, the ratios of the final populations of the A, B, and C states remains unchanged.

Figure 4 shows the normalized fraction of different conformations as a function of activation voltage. Selection and activation of conformer A is first illustrated (top left). As the activation voltage is increased, conformer B begins to form, followed by the transition to

conformer C. Initially conformer B increases to 32% at 25 V activation, however, the fraction of B decreases before leveling off to its quasi-equilibrium population.

Based on these observations, we propose the following for activation of conformer A: as ions are gently heated a fraction of ions converts to conformer B; at higher energies ions have enough energy to overcome the barrier associated with formation of conformer C. In every case, at higher activation voltages a plateau region is reached. In this region we observe that the fractions of A, B, and C are constant (and independent of activation voltage). In the case of the data shown in Figure 4 this region is observed from ~40 to 70 V.

Above ~70 V, we observe the onset of fragment formation (Figure 4, top left). Fragment formation appears to compete directly with all three of the A, B and C states. While we do not show the fragmentation spectra that are generated at high activation voltages it is important to note that inspection of these datasets shows that the ratios of abundant fragment ions appear to be identical (regardless of which state is selected for activation).

All of this information is consistent with the idea that states A, B, and C exist in equilibrium at high activation voltages. This can be highlighted by plotting the fractions of the A, B, and C states together (Figure 4, top right, bottom left, and bottom right, respectively). Here, the fraction of each conformer can be compared from the experiment in which it was selected, to the experiments in which it was formed from the selection of a different conformer. In the equilibrium region, the fractions of A, B, or C are each constant (1.8 ± 0.3%, 16 ± 3%, 80 ± 2%, respectively) regardless of which state was selected for activation.

Activation at different buffer gas pressures

Detailed studies as a function of the activation voltage have been conducted at several different buffer gas pressure settings (ranging from ~1.9 to 4.0 Torr). While we do not discuss this in detail here, we note that the voltage dependence of the features observed after activation varies somewhat depending upon the pressure. As the buffer gas pressure is increased, voltages required to induce structural transitions increase, resulting in a compression of the quasi-equilibrium voltage range. Presumably this is a result of differences that arise in the heating and cooling rates of the ions at different pressures, and is the subject of a future report.90 The overall trends in the features observed are reproduced at different pressures. That is, although the quasi-equilibrium voltage range is compressed, the same fractions of conformers A, B, and C are observed.

Possible origins of transitions

Overall, the data presented above suggests two types of behavior. At low activation voltages it appears that ions overcome barriers between structures and can be converted into other low energy structures. In the cases of A, B, and C it is possible to convert at least some fraction of the population to other states without establishing an equilibrium distribution. This indicates that structures change through specific pathways. Alternatively, when sufficient energy is put into the system the distribution of states becomes independent of the precursor state (or the detailed energy). This indicates that structures A, B, and C are able to interconvert and establish a quasi-equilibrium distribution of states.

It is interesting to consider the origin of those states that are involved in the equilibrium distribution. It is likely that the distribution consists of three types of conformations, varying in shape, charge site assignment, and possibly the structures of the three proline residues. We note that the $[M+2H]^{2+}$ ion exhibits only two features (Figure 2). It is possible that the lower number of resolvable conformations results from a single possible charge-site configuration in which the protons are sequestered at the arginine residues. Recent FAIMS studies have shown evidence for six $[M+2H]^{2+}$ conformations.91

We are currently carrying out detailed molecular modeling studies of these types of structures and our preliminary findings suggest that charge site assignment and cis/trans isomerization of the three proline residues are key factors in the conformational transitions we observe experimentally. Future work will focus on relating the calculated cross sections and stabilities of different trial geometries and charge site configurations to the experimental data.

Conclusions

Ion mobility measurements of the bradykinin $[M+3H]^{3+}$ charge state formed by direct ESI shows evidence for at least six distinct structures. Activation of specific structures shows that at low energies different conformations undergo structural transitions to specific states in a pathway dependent manner. Above a critical activation voltage, all six selected ions yield the same abundances of three conformations (A, B, and C). This suggests that this ratio of states is the gas-phase quasi equilibrium. Some structures (D, E, and F) do not appear to participate in the equilibrium distribution. Presumably these ions have conformations that are established in the presence of solution, and cannot be accessed from the gas-phase in the absence of solvent. The direct observation of an equilibrium distribution of structures, prior to the threshold for dissociation is consistent with the observation of fragmentation spectra that appear essentially indistinguishable for different selected states.

Acknowledgments

This work is supported in part by grants from the National Institutes of Health (1RC1GM090797-01), as well as funding through the DoD NSWC Crane “Next Generation Threat Detection” (N00164-08-C-JQ11).

References

1. Fenn JB, Mann M, Meng CK, Wong SF, Whitehouse CM. Electrospray Ionization for Mass Spectrometry of Large Biomolecules. Science. 1988; 246:64–71. [PubMed: 2675315]
2. Chowdhury SK, Chait BT. Analysis of Mixtures of Closely-Related Forms of Bovine Trypsin by Electrospray Ionization-Mass Spectrometry – Use of Charge State Distributions to Resolve Ions of the Different Forms. Biochem Bioph Res Co. 1990; 173(3):927–931.
3. Katta V, Chait BT. Conformational Changes in Proteins Probed by Hydrogen-Exchange Electrospray Ionization-Mass Spectrometry. Rapid Commun. Mass Sp. 1991; 5(4):214–217.
4. Winger BE, Lightwahl KJ, Rockwood AL, Smith RD. Probing Qualitative Conformation Differences of Multiply Protonated Gas-Phase Proteins via H/D Isotopic Exchange with D_20. J. Am. Chem. Soc. 1992; 114(14):5897–5898.
5. Cheng XH, Fenselau C. Target-Capture and Ion-Molecule Reactions in High-Energy Collisions Between Protonated Polypeptide Ions and Hydrogen-Containing Target Gases. J. Am. Chem. Soc. 1993; 115:10327–10333.
6. Covey TR, Douglas DJ. Collision Cross Sections for Protein Ions. J. Am. Soc. Mass Spectrom. 1993; 4:616–623.
7. Suckau D, Shi Y, Beu SC, Senko MW, Quinn JP, Wampler FM III, McLafferty FW. Coexisting stable conformations of gaseous protein ions. Proc. Natl. Adad. Sci. USA. 1993; 90:790–793.
8. Cox KA, Julian RK Jr. Cooks RG, Kaiser RE Jr. Conformer Selection of Protein Ions by Ion Mobility in a Triple Quadrupole Mass Spectrometer. J. Am. Soc. Mass Spectrom. 1994; 5:127–136.
9. Campbell S, Rodgers MT, Marzluff EM, Beauchamp JL. Deuterium exchange reactions as a probe of biomolecule structure. Fundamental studies of cas phase H/D exchange reactions of protonated glycine oligomers with D_2O, CD_3OD, CD_3CO_2D, and ND_3. J. Am. Chem. Soc. 1995; 117(51): 12840–12854.
10. Clemmer DE, Hudgins RR, Jarrold MF. Naked Protein Conformations: Cytochrome c in the Gas Phase. J. Am. Chem. Soc. 1995; 117:10141–10142.

11. von Helden G, Wyttenbach T, Bowers MT. Conformation of Macromolecules in the Gas Phase: Use of Matrix-Assisted Laser Desorption Methods in Ion Chromatography. Science. 1995; 267:1483–1485. [PubMed: 17743549]
12. Bowers MT, Marshall AG, McLafferty FW. Mass Spectrometry: Recent Advances and Future Directions. J. Phys. Chem. 1996; 100:12897–12910.
13. Smith RD, Bruce JE, Wu Q, Lei QP. New mass spectrometric methods for the study of noncovalent associations of biopolymers. Chem. Soc. Rev. 1997; 26:191–202.
14. Williams ER. Proton Transfer Reactivity of Large Multiply Charged Ions. J. Mass Spectrom. 1996; 31:831–842. [PubMed: 8799309]
15. Loo JA. Studying noncovalent protein complexes by electrospray ionization mass spectrometry. Mass Spectrom. Rev. 1997; 16:1–23. [PubMed: 9414489]
16. Hoaglund Hyzer CS, Counterman AE, Clemmer DE. Anhydrous Protein Ions. Chem. Rev. 1999; 99:3037–3079. [PubMed: 11749510]
17. Wyttenbach T, Bowers MT. Intermolecular interactions in biomolecular systems examined by mass spectrometry. Annu. Rev. Phys. Chem. 2007; 58:511–533. [PubMed: 17129173]
18. Wolynes PG. Biomolecular Folding in Vacuo. Proc. Natl. Acad. Sci.USA. 1995; 92:2426–2427. [PubMed: 7708658]
19. Wood TD, Chorush RA, Wampler FM, Little DP, O'Connor PB, McLafferty FW. Gas-Phase Folding and Unfolding of Cytochrome c Cations. Proc. Natl. Acad. Sci. USA. 1995; 92:2451–2454. [PubMed: 7708663]
20. Valentine SJ, Clemmer DE. H/D Exchange Levels of Shape-Resolved Cytochrome c Conformers in the Gas Phase. J. Am. Chem. Soc. 1997; 119:3558–3566.
21. Schnier PD, Gross DS, Williams ER. Electrostatic Forces and Dielectric Polarizability of Multiply Protonated Gas-Phase Cytochrome c Ions Probed by Ion/Molecule Chemistry. J. Am. Chem. Soc. 1995; 117:6747–6757.
22. Green MK, Lebrilla CB. Ion-Molecule Reactions as Probes of Gas-Phase Structures of Peptides and Proteins. Mass Spectrom. Rev. 1997; 16:53–71. [PubMed: 9414490]
23. Rodriguez-Cruz SE, Klassen JS, Williams ER. Hydration of gas-phase gramicidin S (M+2H)(2+) ions formed by electrospray: The transition from solution to gas-phase structure. J. Mass Spectrom. 1997; 8:565–568.
24. Fye JL, Woenckhaus J, Jarrold MF. Hydration of folded and unfolded gas-phase proteins: Saturation of cytochrome c and apomyoglobin. J. Am. Chem. Soc. 1998; 120:1327–1328.
25. Stephenson JL, Schaaff TG, McLuckey SA. Hydroiodic acid attachment kinetics as a chemical probe of gaseous protein ion structure: Bovine pancreatic trypsin inhibitor. J. Am. Soc. Mass Spectrom. 1999; 10(6):552–556. [PubMed: 10368949]
26. Zubarev RA, Kelleher NL, McLafferty FW. Electron capture dissociation of multiply charged protein cations. A nonergodic process. J. Am. Chem. Soc. 1998; 120:3265–3266.
27. Stephenson JL, McLuckey SA. Ion/ion reactions in the gas phase: Proton transfer reactions involving multiply-charged proteins. J. Am. Chem. Soc. 1996; 118(31):7390–7397.
28. Syka JEP, Coon JJ, Schroeder MJ, Shabanowitz J, Hunt DF. Peptide and protein sequence analysis by electron transfer dissociation mass spectrometry. Proc. Natl. Acad. Sci. U.S.A. 2004; 101:9528–9533. [PubMed: 15210983]
29. Douglas DJ. Applications of Collision Dynamics in Quadrupole Mass Spectrometry. J. Am. Soc. Mass Spectrom. 1998; 9:101–113.
30. Reimann CT, Quist AP, Kopniczky J, Sundqvist BUR, Erlandsson R, Tengvall P. Impacts of Polyatomic Ions on Surfaces – Conformation and Degree of Fragmentation Determined by Lateral Dimensiosn of Impact Features. Nucl. Instrum. Methods Phys. Res.,Sect. B. 1994; 88:29–34.
31. Sullivan PA, Axelsson J, Altmann S, Quist AP, Sundqvist BUR, Reimann CT. Defect formation on surfaces bombarded by energetic multiply charged proteins: Implications for the conformation of gas-phase electrosprayed ions. J. Am. Soc. Mass Spectrom. 1996; 7:329–341.
32. Reimann CT, Sullivan PA, Axelsson J, Quist AP, Altmann S, Roepstorff P, Velazquez I, Tapia O. Conformation of highly-charged gas-phase lysozyme revealed by energetic surface imprinting. J. Am. Chem. Soc. 1998; 120:7608–7616.

33. Wyttenbach T, vonHelden G, Bowers MT. Gas-phase conformation of biological molecules: Bradykinin. J. Am. Chem. Soc. 1996; 118:8355–8364.
34. Shelimov KB, Clemmer DE, Hudgins RR, Jarrold MF. Protein structure in vacuo: Gas-phase confirmations of BPTI and cytochrome c. J. Am. Chem. Soc. 1997; 119:2240–2248.
35. Shelimov KB, Jarrold MF. Conformations, unfolding, and refolding of apomyoglobin in vacuum: An activation barrier for gas-phase protein folding. J. Am. Chem. Soc. 1997; 119:2987–2994.
36. Valentine SJ, Anderson JG, Ellington AD, Clemmer DE. Disulfide-Intact and -Reduced Lysozyme in the Gas Phase: Conformations and Pathways of Folding and Unfolding. J. Phys. Chem. B. 1997; 101:3891–3900.
37. Valentine SJ, Counterman AE, Clemmer DE. Conformer-Dependent Proton-Transfer Reactions of Ubiquitin Ions. J. Am. Soc. Mass Spectrom. 1997; 8:954–961.
38. Johnson RS, Martin SA, Biemann K. Collision-induced fragmentation of $(M + H)^+$ ions of peptides. Side chain specific sequence ions. Int. J. Mass Spectrom. Ion Processes. 1988; 86:137–154.
39. Dongre AR, Jones JL, Somogyi A, Wysocki VH. Influence of peptide composition, gas-phase basicity, and chemical modification on fragmentation efficiency: Evidence for the mobile proton model. J. Am. Chem. Soc. 1996; 118:8365–8374.
40. Vachet RW, Asam MR, Glish GL. Secondary interactions affecting the dissociation patterns of arginine-containing peptide ions. J. Am. Chem. Soc. 1996; 118:6252–6256.
41. Loo JA, Edmonds CG, Smith RD. Primary Sequence Information from Intact Proteins by Electrospray Ionization Tandem Mass-Spectrometry. Science. 1990; 248:201–204. [PubMed: 2326633]
42. Wu Q, Van Orden S, Cheng X, Bakhtiar R, Smith RD. Characterization of Cytochrome c Variants with High-Resolution FTICR Mass-Spectrometry – Correlation of Fragmentation and Structure. Anal. Chem. 1995; 67:2498. [PubMed: 8686880]
43. Mack E. Average Cross-Sectional Areas of Molecules by Gaseous Diffusion Methods. J. Am. Chem. Soc. 1925; 47:2468–2482.
44. Revercomb HE, Mason EA. Theory of Plasma Chromatography Gaseous Electrophoresis - Review. Anal. Chem. 1975; 47:970–983.
45. Mason, EA.; McDaniel, EW. Transport Properties of Ions in Gases. Wiley; New York: 1988.
46. St. Louis RH, Hill HH. Ion Mobility Spectrometry in Analytical Chemistry. Crit. Rev. Anal. Chem. 1990; 21:321–355. For a review of IMS techniques see (and references therein).
47. Clemmer DE, Jarrold MF. Ion Mobility Measurements and their Applications to Clusters and Biomolecules. J. Mass Spectrom. 1997; 32:577–592. For a review of IMS techniques see (and references therein).
48. Bohrer BC, Merenbloom SI, Koeniger SL, Hilderbrand AE, Clemmer DE. Biomolecule Analysis by Ion Mobility Spectrometry. Annu. Rev. Anal. Chem. 2008; 1(10):1–10. For a review of IMS techniques see (and references therein).
49. Shvartsburg AA, Jarrold MF. An exact hard-spheres scattering model for the mobilities of polyatomic ions. Chem. Phys. Lett. 1996; 261:86–91.
50. Mesleh MF, Hunter JM, Shvartsburg AA, Schatz GC, Jarrold MF. Structural information from ion mobility measurements: effects of the long-range potential. J. Phys. Chem. 1996; 100:16082–86.
51. Wyttenbach T, von Helden G, Batka JJ, Carlat D, Bowers MT. Effect of the long-range potential on ion mobility measurements. J. Am. Chem. Soc. 1997; 8:275–82.
52. Hudgins RR, Ratner MA, Jarrold MF. Design of Helices That Are Stable in Vacuo. J. Am. Chem. Soc. 1998; 120:12974–12975.
53. Wyttenbach T, Bushnell JE, Bowers MT. Salt Bridge Structures in the Absence of Solvent? The Case for the Oligoglycines. J. Am. Chem. Soc. 1998; 120:5098–5103.
54. Counterman AE, Clemmer DE. Compact -> Extended Helix Transitions of Polyalanine in Vacuo. J. Phys. Chem. B. 2003; 107:2111–2117.
55. Ruotolo BT, Verbeck GF, Thomson LM, Gillig KJ, Russell DH. Observation of conserved solution-phase secondary structure in gas-phase tryptic peptides. J. Am. Chem. Soc. 2002; 124(16):4214–4215. [PubMed: 11960442]

56. Myung S, Badman E, Lee YJ, Clemmer DE. Structural Transitions of Electrosprayed Ubiquitin Ions Stored in an Ion Trap over ~10 ms to 30s. J. Phys. Chem. A. 2002; 106:9976–9982.
57. Badman E, Myung S, Clemmer DE. Evidence for Unfolding and Refolding of Gas Phase Cyctrochrome c Ions in a Paul Trap. J. Am. Soc. Mass Spectrom. 2005; 16:1493–1497. [PubMed: 16019223]
58. Koeniger SL, Merenbloom SI, Clemmer DE. Evidence for Many Resolvable Structures within Conformation Types of Electrosprayed Ubiquitin Ions. J. Phys. Chem B. 2006; 110:7017–7021. [PubMed: 16571016]
59. Jarrold MF. Unfolding, Refolding, and Hydration of Proteins in the Gas Phase. Acc. Chem. Res. 1999; 32:360–367.
60. Valentine SJ, Clemmer DE. Temperature Dependent H/D Exchange of Compact and Elongated Cytochrome c Ions in the Gas Phase. J. Am. Soc. Mass Spectrom. 2002; 13:506–517. [PubMed: 12019975]
61. Loo JA, He JX, Cody WL. Higher Order Structure in the Gas Phase Reflects Solution Structure. J. Am. Chem. Soc. 1998; 120:4542–4543.
62. Hudgins RR, Woenckhaus J, Jarrold MF. High Resolution Ion Mobility Measurements for Gas-Phase Proteins: Correlation Between Solution Phase and Gas Phase Conformations. Int. J. Mass Spectrom. Ion Processes. 1997; 165/166:497–507.
63. Li J, Taraszka JA, Counterman AE, Clemmer DE. Influence of solvent composition and capillary temperature on the conformations of electrosprayed ions: unfolding of compact ubiquitin conformers from pseudonative and denatured solutions. Int. J. Mass. Spectrom. 1999; 185/186/187:37–47.
64. Ruotolo BT, Giles K, Campuzano I, Sandercock AM, Bateman RH, Robinson CV. Evidence for Macromolecular Protein Rings in the Absence of Bulk Water. Science. 2005; 310:1658–1661. [PubMed: 16293722]
65. Painter AJ, Jaya N, Basha E, Vierling E, Robinson CV, Benesch JLP. Real-Time Monitoring of Protein Complexes Reveals their Quaternary Organization and Dynamics. Chemistry & Biology. 2008; 15:246–253. [PubMed: 18355724]
66. Bernstein SL, Dupuis NF, Lazo ND, Wyttenbach T, Condron MM, Bitan G, Teplow DB, Shea JE, Ruotolo BT, Robinson CV, Bowers MT. Amyloid-beta protein oligomerization and the importance of tetramers and dodecamers in the aetiology of Alzheimer's disease. Nat. Chem. 2009; 1(4):326–331. [PubMed: 20703363]
67. Kaltashov IA, Fabris D, Fenselau CC. Assessment of Gas-Phase Basicities of Protonated Petides by the Kinetic Method. J. Phys. Chem. 1995; 99(24):10046–10051.
68. Dongre AR, Jones JL, Somogyi A, Wysocki VH. Influence of Peptide Composition, Gas-Phase Basicity, and Chemical Modification on Fragmentation Efficiency: Evidence for the Mobile Proton Model. J. Am. Chem. Soc. 1996; 118:8365–8374.
69. Schnier PD, Price WD, Jockusch RA, Williams ER. Blackbody infrared radiative dissociation of bradykinin and its analogues: Energetics, dynamics, and evidence for salt-bridge structures in the gas phase. J. Am. Chem. Soc. 1996; 118(30):7178–7189. [PubMed: 16525512]
70. Wyttenbach T, Bowers MT. Gas phase conformations of biological molecules: The hydrogen/deuterium exchange mechanism. J. Am. Soc. Mass Spectrom. 1999; 10(1):9–14.
71. Schnier PD, Williams ER. Analysis of isomeric mixtures using blackbody infrared radiative dissociation: Determining isomeric purity and obtaining individual tandem mass spectra simultaneously. Anal. Chem. 1998; 70(14):3033–3041. [PubMed: 9684551]
72. Countermann AE, Valentine SJ, Srebalus CA, Henderson SC, Hoaglund CS, Clemmer DE. High-Order Structure and Dissociation of Gaseous Peptide Aggregates that are Hidden in Mass Spectra. J. Am. Soc. Mass Spectrom. 1998; 9:743–759. [PubMed: 9692251]
73. Butcher DJ, Asano KG, Goeringer DE, McLuckey SA. Thermal Dissociation of Gaseous Bradykinin Ions. J. Phys. Chem. A. 1999; 103:8664–8671.
74. Gimon-Kinsel RE, Barbacci DC, Russell DH. Conformations of protonated gas-phase bradykinin ions: Evidence for intramolecular hydrogen bonding. J. Mass Spectrom. 1999; 34(2):124–136. [PubMed: 10093213]

75. Guo Y, Wang J, Javahery G, Thomson BA, Siu KW. M. Ion Mobility Spectrometer with Radial Collisional Focusing. Anal. Chem. 2005; 77:266–275. [PubMed: 15623305]
76. Herrmann KA, Kuppannan K, Wysocki VH. Fragmentation of doubly-protonated peptide ion populations labeled by H/D exchange with CD3OD. Int. J. Mass Spectrom. 2006; 249:93–105. [PubMed: 18802500]
77. Rodriguez CF, Orlova G, Guo Y, Li X, Siu C–K, Hopkinson AC, Siu KWM. Gaseous Bradykinin and Its Singly, Doubly, and Triply Protonated Forms: A First-Principles Study. J. Phys. Chem. B. 2006; 110(14):7528–7537. [PubMed: 16599534]
78. Chen H, Eberlin LS, Cooks RG. Neutral fragment mass spectra via ambient thermal dissociation of peptide and protein ions. J. Am. Chem. Soc. 2007; 129(18):5880–5886. [PubMed: 17432855]
79. Fernandez-Lima FA, Wei H, Gao YQ, Russell DH. On the Structure Elucidation Using Ion Mobility Spectrometry and Molecular Dynamics. J. Phys Chem. A. 2009; 113(29):8221–8234. [PubMed: 19569657]
80. Wittmer D, Luckenbill BK, Hill HH, Chen YH. Electrospray Ionization Ion Mobility Spectrometry. Anal. Chem. 1994; 66:2348–2355.
81. Gillig KJ, Ruotolo B, Stone EG, Russell DH, Fuhrer K, Gonin M, Schultz AJ. Coupling High-Pressure MALDI with Ion Mobility/Orthogonal Time-of Flight Mass Spectrometry. Anal. Chem. 2000; 72:3965–3971. [PubMed: 10994952]
82. Hoaglund CS, Valentine SJ, Sporleder CR, Reilly JP, Clemmer DE. Three-Dimensional Ion Mobility/TOFMS Analysis of Electrosprayed Biomolecules. Anal. Chem. 1998; 70:2236–2242. [PubMed: 9624897]
83. Hoaglund-Hyzer CS, Li J, Clemmer DE. Mobility Labeling for Parallel CID of Ion Mixtures. Anal. Chem. 2000; 72:2737–2740. [PubMed: 10905301]
84. Valentine SJ, Kulchania M, Barnes CAS, Clemmer DE. Multidimensional Separations of Complex Peptide Mixtures: A Combined High-Performance Liquid Chromatography/Ion Mobility/Time-of-Flight Mass Spectrometry Approach. Int. J. Mass Spectrom. 2001; 212:97–109.
85. Tang K, Shvartsburg AA, Lee HN, Prior DC, Buschbach MA, Li FM, Tolmachev AV, Anderson GA, Smith RD. High-Sensitivity Ion Mobility Spectrometry/Mass Spectrometry Using Electrodynamic Ion Funnel Interfaces. Anal. Chem. 2005; 77:3330–3339. [PubMed: 15889926]
86. Koeniger SL, Merenbloom SI, Valentine SJ, Jarrold MF, Udseth HR, Smith RD, Clemmer DE. An IMS-IMS Analogue of MS-MS. Anal. Chem. 2006; 78:4161–4174. [PubMed: 16771547]
87. Merenbloom SI, Koeniger SL, Valentine SJ, Plasencia MD, Clemmer DE. IMS-IMS and IMS-IMS-IMS/MS for Separating Peptide and Protein Fragment Ions. Anal. Chem. 2006; 78:2802–2809. [PubMed: 16615796]
88. a Shaffer SA, Tang KQ, Anderson GA, Prior DC, Udseth HR, Smith RD. A Novel Ion Funnel for Focusing Ions at Elevated Pressure Using Electrospray Ionization Mass Spectrometry. Rapid Commun. Mass Spectrom. 1997; 11:1813–1817. b Shaffer SA, Prior DC, Anderson GA, Udseth HR, Smith RD. An Ion Funnel Interface for Improved Ion Focusing and Sensitivity Using Electrospray Ionization Mass Spectrometry. Anal. Chem. 1998; 70:4111–4119. [PubMed: 9784749]
89. Counterman AE, Hilderbrand AE, Srebalus Barnes CA, Clemmer DE. Formation of Peptide Aggregates during ESI: Size, Charge, Composition, and Contributions to Noise. J. Am. Soc. Mass Spectrom. 2001; 12:1020–1035.
90. Pierson, NA.; Clemmer, DE. (manuscript in preparation)
91. Shvartsburg AA, Li F, Tang K, Smith RD. High-Resolution FAIMS Using New Planar Geometry Analyzers. Anal. Chem. 2006; 78:3706–3714. [PubMed: 16737227]

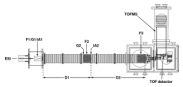

Figure 1.
Schematic diagram of the IMS–IMS-TOF instrument used to select and activate conformations of bradykinin $[M+3H]^{3+}$ions. The instrument consists of an ESI source, a 1.8-meter drift tube (D1 and D2), and a time-of-flight mass spectrometer. See text for details.

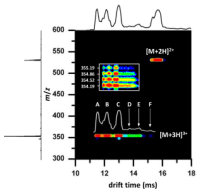

Figure 2.

Two-dimensional nested drift time(*m*/*z*) plot showing the $[M+2H]^{2+}$ and $[M+3H]^{3+}$ charge states of bradykinin. The total ion drift time distribution shown across the top is obtained by integrating across the entire *m*/*z* range for each given drift time. The mass spectrum shown on the left is obtained by integrating across all drift times for each *m*/*z* value. The $[M+3H]^{3+}$ conformation assignments of A, B, C, D, E, and F are shown in the drift distribution above the 2D features. The inset shows an expansion of the *m*/*z* axis in the *m*/*z* 354 region; the isotopic distribution of the bradykinin $[M+3H]^{3+}$ ions is shown. The data were collected using a He buffer gas pressure of ~3.0 Torr.

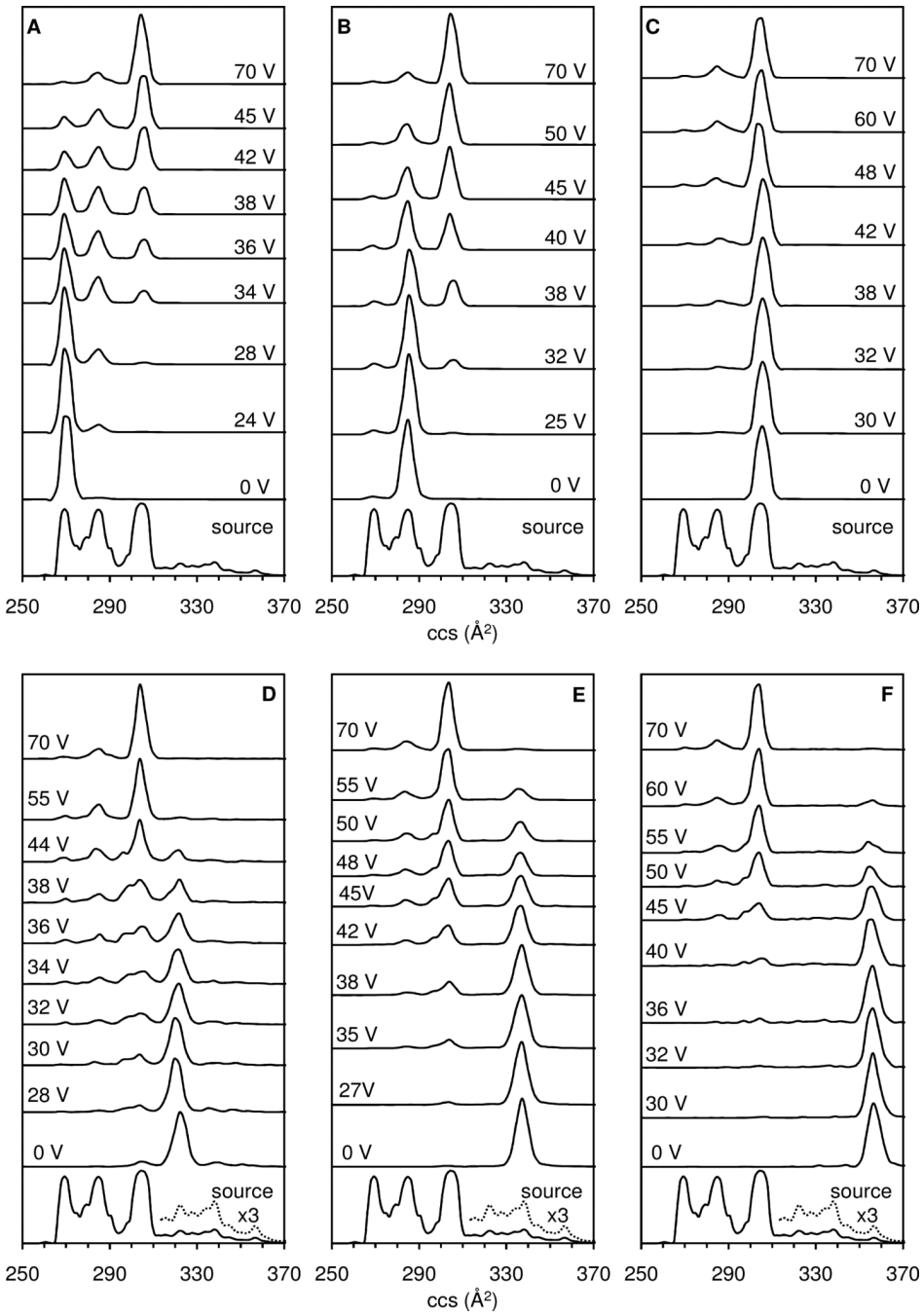

Figure 3.

Drift profiles of the $[M+3H]^{3+}$ bradykinin ion plotted on a collision cross section scale. The bottom trace in each panel shows the ESI source distribution obtained for the dataset shown in Figure 2. The intensity of a portion of the ESI source distribution is multiplied by a factor of 3 in the bottom panels to show the features corresponding to conformations D, E, and F. Each panel shows one of six separate experiments (A-F) beginning with the initial selection (no activation) followed by increasing activation voltages up to 70 V. The areas under the selection and activation collision cross section distributions are normalized to unity. For the selection experiments represented in this Figure, the He buffer gas pressure was maintained

at ~1.9 Torr. Selections of conformations A through F all converge to the same quasi-equilibrium distribution of A, B, and C at 70 V. See text for discussion.

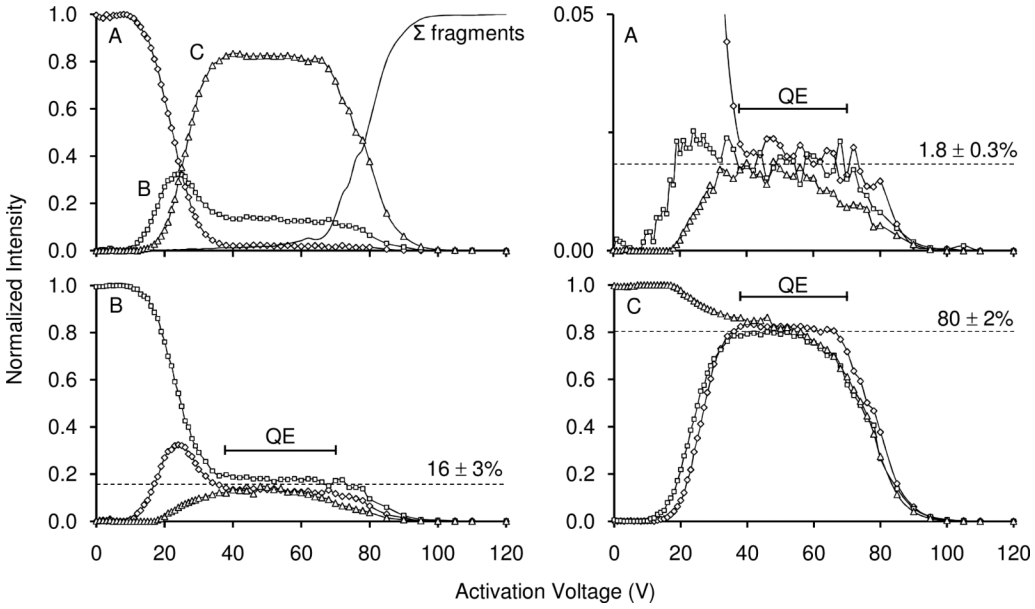

Figure 4.

Normalized intensity as a function of activation voltage for selection of conformer A converting to conformers B and C, and fragmenting (top left). Here open circles, open squares, and open triangles represent the normalized intensities of conformations A, B, and C, respectively at the given activation voltages. The solid line represents the normalized intensity of all observed fragments originating from the selected ions. Normalized intensities of conformation A selected, A made from the selection of conformation B, and A made from the selection of conformation C are shown in the top right spectrum. The symbols for each conformation are the same as given above. Similarly, intensities for conformation B and conformation C (selected and formed) are shown in the bottom left and the bottom right plots, respectively. The bracketed line above 38-64 V denotes the quasi-equilibrium (QE) region prior to fragmentation. The dashed line denotes the average for each conformation at equilibrium. See text for discussion. Data for these plots were obtained from experiments performed using a He buffer gas pressure of ~3.0 Torr.

Table 1

Collision cross sections obtained for the six $[M+3H]^{3+}$ bradykinin conformations.

Conformation[a]	ccs (Å^2)[b]	% abundance (source)[c]	% abundance (QE)[d]
A	269 (275[e])	22.1%	1.8 ± 0.3%
B	285 (284[f], 293[e])	31.4%	16 ± 3%
C	305	30.8%	80 ± 2%
D	322	4.3%	< 1%
E	338	4.7%	< 1%
F	356	1.9%	< 1%

[a] Conformations from highest to lowest mobilities are shown in Figure 2.

[b] Collision cross sections are reported using drift times from peak maxima in the overall arrival time distribution of $[M+3H]^{3+}$ bradykinin ions.

[c] Percent relative abundance (peak area) of each conformation relative to the total $[M+3H]^{3+}$ source distribution.

[d] Percent relative abundance (peak area) of each conformation relative to the total $[M+3H]^{3+}$ distribution in the QE range.

[e] Published experimental collision cross section from reference 75.

[f] Published experimental collision cross section from reference 72.